Time-varying Injection Shift Factors to Predict Post-contingency Dynamic Line Flows

Abdullah Al-Digs[†], Sairaj V. Dhople[‡], Yu Christine Chen[§]
[†§]Department of Electrical and Computer Engineering, The University of British Columbia, Canada
[‡]Department of Electrical and Computer Engineering, University of Minnesota, Twin Cities, USA
Email: [†]aldigs@ece.ubc.ca, [‡]sdhople@umn.edu, [§]chen@ece.ubc.ca

***Abstract*—In this paper, we derive analytical closed-form expressions for time-varying generator participation factors that are valid throughout the post-contingency transient period. Combining these with conventional injection shift factors (ISFs) computed at the pre-disturbance steady-state operating point, post-contingency dynamic transmission-line flows after the outage of any one particular asset, such as a generator or load, can be accurately predicted. This is advantageous over conventional ISF-based contingency analysis, which is applicable only for the post-disturbance steady-state operating point. As such, operators can determine whether or not any transmission lines exceed their operational limits during the transient without repeated time-domain simulations for each credible contingency. We validate the proposed methodology via numerical case studies conducted on standard IEEE test systems.**

I. Introduction

This paper presents analytical closed-form expressions for time-domain functions that uncover the mapping from a generation-load imbalance to the active-power flow on a line in the network. We refer to these as *time-varying injection shift factors* (TVISFs). These are extensions to the well-known *injection shift factors* (ISFs) [1]—which indicate whether or not the system is $N-1$ secure at a post-disturbance steady state—to the entire time period capturing the evolution of the post-disturbance generator dynamics to the new steady state. The ISFs are computed by linearizing the power-flow equations around a particular operating point, and they specify the sensitivities of line active-power flows with respect to variations in the active-power injection (generation or load) at a particular bus.

In order to yield meaningful line-flow predictions, ISFs must be used in conjunction with particular power allocation schemes, which are based on the idea of a distributed slack bus where any system power imbalance is absorbed by injections at several buses with different participation factors. These participation factors can be chosen based on economic dispatch results to minimize generation cost; they can also be gleaned from insights obtained based on post-contingency transient generator dynamics. Conventionally, each set of participation factors corresponds to the power allocation scheme for all generators for a particular snapshot in time. On the other hand, the proposed TVISFs are derived by systematically augmenting ISFs with time-domain functions that uncover the mapping between generator outputs and the load disturbance—essentially, time-varying power allocation participation factors that indicate the proportion contributed by each generator to restore system generation-load balance. This is done with the aid of a reduced-order system frequency response model assuming all the buses have the same frequency even during transients [2].

Traditionally, ISFs (in conjunction with constant participation factors) have been used exclusively to predict transmission-line flows at the post-disturbance steady state after a load change, and to verify that the steady-state operational reliability requirements are met [1], [3]–[5]. Thus, conventional ISF-based contingency analysis yields little to no insight during the transient period before steady state is reached. The proposed TVISFs provide an analytical solution precisely to this problem. In so doing, they offer a compelling solution to computationally efficient dynamic contingency analysis, which is typically accomplished by performing repeated time-domain simulations of a full-order dynamical model of the system [6].

The remainder of this paper is organized as follows. Section II describes conventional ISFs and subsequently outlines the problem statement. In Section III, we derive the proposed TVISFs by developing several auxiliary and approximate system dynamical models. The resulting TVISFs are verified via numerical case studies in Section IV. Finally, Section V offers concluding remarks and directions for future work.

II. Preliminaries

Our goal is to predict the change in line active-power flow corresponding to a change in nodal active-power injection over the transient period experienced after the disturbance. Along the time scales relevant to this work, dynamics of synchronous generator $g \in \mathcal{G}$, which denotes the set of generators in the system, can be modelled as follows. For each generator $g \in \mathcal{G}$, let $\omega_g(t)$, $P_g^{\rm m}(t)$, and $P_g(t)$ denote its rotor electrical angular speed, turbine mechanical power, and electrical-power output, respectively. Assume each generator initially operates at the steady-state equilibrium point with $\omega_g(0) = \omega_{\rm s} = 2\pi 60\,\text{rad/s}$, the synchronous frequency. Defining $\Delta\omega_g := \omega_g - \omega_{\rm s}$, dynamics of generator $g \in \mathcal{G}$ can be described by

$$\begin{aligned} M_g \Delta\dot{\omega}_g(t) &= P_g^{\rm m}(t) - D_g \Delta\omega_g(t) - P_g(t), \\ \tau_g \dot{P}_g^{\rm m}(t) &= P_g^{\rm r} - P_g^{\rm m}(t) - R_g^{-1}\Delta\omega_g(t), \end{aligned} \tag{1}$$

where M_g and D_g denote, respectively, the inertia constant and damping coefficient; and τ_g, P_g^{r}, and R_g denote the governor time constant, reference power input, and droop constant, respectively.

A. Conventional Injection Shift Factors

The injection shift factor (ISF) quantifies the redistribution of power through each transmission line following a change in generation or load on a particular bus. Let $\mathcal{N}$ denote the set of buses in the system, and let $\mathcal{E}$ denote the set of transmission lines. The ISF of line $(m,n) \in \mathcal{E}$ with respect to bus k, denoted by $\Gamma^k_{(m,n)}$, is the linear sensitivity of the active-power flow in line (m,n) with respect to the active-power injection at bus k. The change in active-power flow in line (m,n), denoted by $\Delta P_{(m,n)}(t)$, due to small variations in bus active-power injections, denoted by $\Delta P_k(t)$, can be approximated as

$$\Delta P_{(m,n)}(t) = \sum_k \Gamma^k_{(m,n)} \Delta P_k(t), \tag{2}$$

where $\sum_k \Delta P_k(t) = 0$ (neglecting losses).

Consider the change in flow in line (m,n) when the active-power demand at load bus ℓ increases by ΔP_{load} at time $t = 0$, i.e., $P_\ell(t) = P_\ell(0) + \Delta P_{\mathrm{load}}$, $t > 0$. Leveraging the relationship in (2), this scenario can be described by

$$\Delta P_{(m,n)}(t) = \sum_{g \in \mathcal{G}} \Gamma^g_{(m,n)} \Delta P_g(t) - \Gamma^\ell_{(m,n)} \Delta P_{\mathrm{load}}, \tag{3}$$

where $\Delta P_g(t)$ represents the change in generator g output as a result of the disturbance, and $\sum_g \Delta P_g = \Delta P_{\mathrm{load}}$. Ostensibly, there are infinitely many allocation schemes for generators in the system to respond to this generation-load mismatch, each leading to different predicted line flows. For a particular snapshot at time t, the power allocation scheme for each $g \in \mathcal{G}$ is expressed as

$$\Delta P_g(t) = f_{P_g}(t) \Delta P_{\mathrm{load}}, \tag{4}$$

where $\sum_{g \in \mathcal{G}} f_{P_g}(t) = 1$. The participation factors $f_{P_g}(t)$'s can take values based on insights gleaned from economic dispatch, governor control, or synchronous generator inertia characteristics [7]. For example, inertia- and governor-based participation factors are obtained by defining

$$f_{P_g} = \frac{M_g}{\sum_{k \in \mathcal{G}} M_k}, \quad f_{P_k} = \frac{R_g^{-1}}{\sum_{k \in \mathcal{G}} R_k^{-1}}, \tag{5}$$

respectively. The participation factors in (5) describe realizations of the distributed slack bus based on power-frequency characteristics of generators in the system [7]. Next, we illustrate the ideas introduced above via a numerical example.

Example 1 (Three-bus System): Consider the three-bus lossless system with one-line diagram shown in Fig. 1. Pertinent network parameters and pre-disturbance initial conditions are detailed in Appendix A. The initial steady-state active-power flows in lines $(1,2)$, $(2,3)$, and $(1,3)$ are $P_{(1,2)}(t) = 0.042\,\mathrm{p.u.}$, $P_{(2,3)}(t) = 0.833\,\mathrm{p.u.}$, and $P_{(1,3)}(t) = 1.517\,\mathrm{p.u.}$, respectively. Suppose the bus 3 load

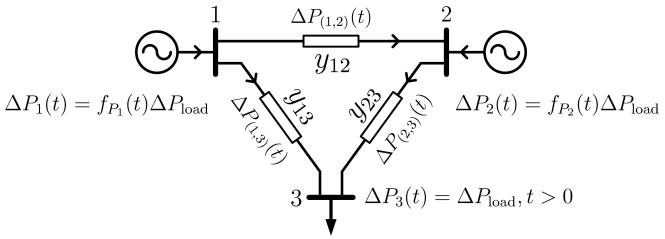

Fig. 1: Network topology for three-bus system.

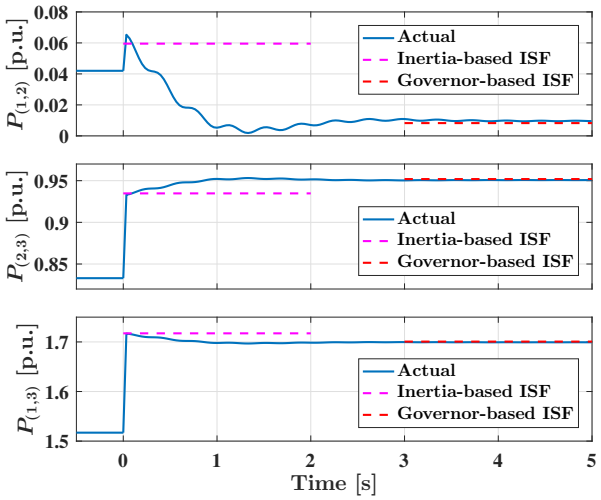

Fig. 2: Line active-power flows in three-bus system due to 0.3 p.u. increase in active-power demand at bus 3.

experiences a step increase of 0.3 p.u. at $t = 0\,\mathrm{s}$, and generators in the system respond dynamically to this mismatch. Pre- and post-disturbance line flows are obtained via time-domain simulations in PSAT [8] and subsequently plotted in Fig. 2.

We also predict line flows using ISFs in conjunction with inertial- and governor-based participation factors in (5) due to the load increase. Based on parameter values listed in Appendix A, the inertia-based participation factors for the synchronous generators are $f_{P_1} = 8/11.01$ and $f_{P_2} = 3.01/11.01$. Substituting these participation factors into (4), we predict how the load increase is allocated between the two generators based on their inertial characteristics. Then, using (3), this inertia-based allocation corresponds to line-flow changes of $\Delta P_{(1,2)} = 0.0175\,\mathrm{p.u.}$, $\Delta P_{(2,3)} = 0.1017\,\mathrm{p.u.}$, and $\Delta P_{(1,3)} = 0.2\,\mathrm{p.u.}$ Similarly, the governor-based participation factors $f_{P_1} = f_{P_2} = 1/2$ help to predict steady-state line-flow changes as $\Delta P_{(1,2)} = -0.0337\,\mathrm{p.u.}$, $\Delta P_{(2,3)} = 0.1189\,\mathrm{p.u.}$, and $\Delta P_{(1,3)} = 0.184\,\mathrm{p.u.}$ These predicted quantities are superimposed onto the actual line-flow dynamics in Fig. 2. Indeed, we notice that the inertia-based ISFs provide adequate line-flow predictions shortly after the load disturbance, and the governor-based ISFs yield satisfactory line-flow estimates over slower time scales.

While inertia- and governor-based participation factors offer some intuition for predicting dynamic line flows, as shown in Fig. 2, they do not fully describe the transient

behaviour of generators. In light of this, we extend the single-snapshot participation factors into time-varying functions that delineate how the generation-load mismatch is allocated amongst generators over the entire transient period prior to reaching the post-disturbance steady state. ■

B. Problem Statement

To capture the mapping between the time-varying generator response to the load change, we acknowledge the dynamics of generators in (1) and seek an explicit closed-form time-domain function for the participation factor $f_{P_g}(t)$. With this in place, substituting (4) into (3), we formally define the *time-varying injection shift factor* from bus ℓ to line (m,n) as

$$\gamma^{\ell}_{(m,n)}(t) := \sum_{g\in\mathcal{G}} \Gamma^{g}_{(m,n)} f_{P_g}(t) - \Gamma^{\ell}_{(m,n)}, \tag{6}$$

with which we can express

$$\Delta P_{(m,n)}(t) = \gamma^{\ell}_{(m,n)}(t)\Delta P_{\text{load}}. \tag{7}$$

The functions $f_{P_g}(t)$ can be obtained in analytical closed form from a suitable reduced-order model. We discuss this next.

III. Deriving Time-varying Injection Shift Factors

This section outlines several auxiliary and approximate models that facilitate the derivation of TVISFs before delving into the solution approach.

A. Auxiliary Models

In order to derive analytical closed-form expressions for TVISFs, we will find it useful to define several approximate models, which are detailed below.

1) Common-frequency Generator Dynamical Model: Assume common frequency for the model in (1), i.e., $\Delta\omega_g = \Delta\omega$, $\forall g \in \mathcal{G}$, then the dynamics of each generator g can be expressed as

$$M_g\Delta\dot{\omega}(t) = P^{\text{m}}_g(t) - D_g\Delta\omega(t) - P_g(t), \tag{8}$$

$$\tau_g\dot{P}^{\text{m}}_g(t) = P^{\text{r}}_g - P^{\text{m}}_g(t) - R^{-1}_g\Delta\omega(t). \tag{9}$$

Summing (8) over all $g \in \mathcal{G}$ we get

$$M_{\text{eff}}\Delta\dot{\omega}(t) = \sum_{g\in\mathcal{G}} P^{\text{m}}_g(t) - D_{\text{eff}}\Delta\omega(t) - P_{\text{load}}(t), \tag{10}$$

where the total electrical load is $P_{\text{load}} := \sum_{g\in\mathcal{G}} P_g$, the *effective inertia constant*, $M_{\text{eff}} := \sum_{g\in\mathcal{G}} M_g$, and *effective damping constant*, $D_{\text{eff}} = \sum_{g\in\mathcal{G}} D_g$. Furthermore, collecting copies of (9) $\forall g \in \mathcal{G}$, we can write

$$\text{diag}(\tau)\dot{P}^{\text{m}}(t) = P^{\text{r}} - P^{\text{m}}(t) - R^{-1}\Delta\omega(t), \tag{11}$$

where we define:[1]

$$\begin{aligned} &\tau := [\tau_1,\ldots,\tau_{|\mathcal{G}|}]^{\text{T}},\ R^{-1} := [R_1^{-1},\ldots,R_{|\mathcal{G}|}^{-1}]^{\text{T}},\\ &P^{\text{m}} := [P_1^{\text{m}},\ldots,P_{|\mathcal{G}|}^{\text{m}}]^{\text{T}},\ P^{\text{r}} := [P_1^{\text{r}},\ldots,P_{|\mathcal{G}|}^{\text{r}}]^{\text{T}}. \end{aligned} \tag{12}$$

[1]The notation adopted for the vector collecting the speed-droop regulation constants is motivated by the desire to retain consistency.

Combining (10) and (11), we get the state-space model:

$$\dot{x} = Ax + Bu. \tag{13}$$

The state vector and input, $x, u \in \mathbb{R}^{|\mathcal{G}|+1}$, and system matrices, $A, B \in \mathbb{R}^{|\mathcal{G}|+1\times|\mathcal{G}|+1}$ are given by

$$\begin{aligned} &x = [\Delta\omega, (P^{\text{m}})^{\text{T}}]^{\text{T}}, \quad u = [P_{\text{load}}, (P^{\text{r}})^{\text{T}}]^{\text{T}}, \\ &A = \begin{bmatrix} -M_{\text{eff}}^{-1}D_{\text{eff}} & M_{\text{eff}}^{-1}1^{\text{T}}_{|\mathcal{G}|} \\ -A_R & -A_\tau \end{bmatrix},\ B = \text{diag}\{-M_{\text{eff}}^{-1}, A_\tau\}, \end{aligned} \tag{14}$$

where $A_\tau := \text{diag}(\tau)^{-1}$ and $A_R := A_\tau R^{-1}$.

2) Reduced-order System Model: Consider the following second-order model to capture the frequency dynamics:

$$\dot{\overline{x}} = \overline{A}\overline{x} + \overline{B}\overline{u}. \tag{15}$$

The state vector and input, $\overline{x}, \overline{u} \in \mathbb{R}^2$, and system matrices, $\overline{A}, \overline{B} \in \mathbb{R}^{2\times 2}$ are given by

$$\begin{aligned} &\overline{x} = [\Delta\overline{\omega}, \overline{P}^{\text{m}}]^{\text{T}}, \qquad \overline{u} = [P_{\text{load}}, \overline{P}^{\text{r}}]^{\text{T}}, \\ &\overline{A} = \begin{bmatrix} -M_{\text{eff}}^{-1}D_{\text{eff}} & M_{\text{eff}}^{-1} \\ -\overline{\tau}^{-1}R_{\text{eff}}^{-1} & -\overline{\tau}^{-1} \end{bmatrix},\ \overline{B} = \begin{bmatrix} -M_{\text{eff}}^{-1} & 0 \\ 0 & \overline{\tau}^{-1} \end{bmatrix}, \end{aligned} \tag{16}$$

where $\overline{\tau} > 0$ represents the time constant of the aggregated governor in the reduced-order model, $\overline{P}^{\text{m}}$ is the mechanical power of the aggregate model, and

$$\overline{P}^{\text{r}} = \sum_{g\in\mathcal{G}} P^{\text{r}}_g, \quad R^{-1}_{\text{eff}} = \sum_{g\in\mathcal{G}} R^{-1}_g. \tag{17}$$

Various options have been proposed for $\overline{\tau}$ in the literature. The average of all entries in τ is utilized in [9], [10]. However, this does not yield any guarantees on the error in trajectories generated by the original model (13) and the reduced-order model (15). On the other hand, the choice

$$\overline{\tau} = \arg\min_{\widehat{\tau}\geq 0} \|(\Gamma(\widehat{\tau}) - I_{|\mathcal{G}|+1})A\|_2, \tag{18}$$

where $\Gamma(\widehat{\tau}) := \text{diag}\{1, \widehat{\tau}^{-1}\text{diag}(\tau)\}$ as suggested in [11] yields a rigorous error bound on $|\Delta\omega(t) - \Delta\overline{\omega}(t)|$. Note that when all entries of τ are identical, the matrix $\Gamma(\widehat{\tau})$ reduces to the identity matrix and (18) returns the average of entries of τ.

3) Approximate Generator Dynamical Model: Using $\Delta\overline{\omega}$ from (15) as a proxy for $\Delta\omega$ in (8)–(9), define the auxiliary dynamical model for generator $g \in \mathcal{G}$

$$\tau_g\dot{\overline{P}}^{\text{m}}_g(t) = P^{\text{r}}_g - \overline{P}^{\text{m}}_g(t) - R^{-1}_g\Delta\overline{\omega}(t), \tag{19}$$

$$\overline{P}_g(t) = \overline{P}^{\text{m}}_g(t) - D_g\Delta\overline{\omega}(t) - M_g\Delta\dot{\overline{\omega}}(t). \tag{20}$$

Since $\Delta\omega(t) \approx \Delta\overline{\omega}(t)$, it follows that $\overline{P}_g(t) \approx P_g(t)$. This is pertinent, since unlike $P_g(t)$, $\overline{P}_g(t)$ can be obtained in analytical closed form (leveraging the second-order model in (15) and the auxiliary model (19)–(20)) as a function of the load disturbance. In other words, with the aid of the reduced-order and auxiliary dynamical models, an approximation to the function $f_{P_g}(t)$ in (6) can be obtained in analytical closed form. We outline this next.

B. Solution Strategy to Obtain $f_{P_g}(t)$

Define deviations $\Delta\overline{P}_g(t) = \overline{P}_g(t) - \overline{P}_g(0)$, $\Delta\overline{P}^{\mathrm{m}}_g(t) := \overline{P}^{\mathrm{m}}_g(t) - \overline{P}^{\mathrm{m}}_g(0)$, $\Delta\overline{P}^{\mathrm{m}}(t) := \overline{P}^{\mathrm{m}}(t) - \overline{P}^{\mathrm{m}}(0)$ that occur due to a step change in the load at time $t = 0$ of ΔP_{load}, so that $P_{\mathrm{load}}(t) = P_{\mathrm{load}}(0) + \Delta P_{\mathrm{load}}$, $t > 0$. The transfer functions from the load to frequency offset and the aggregated governor mechanical power as suggested by (15) are:

$$\begin{aligned}\frac{\Delta\overline{\omega}(s)}{P_{\mathrm{load}}(s)} &= -\frac{k(s+\zeta)}{s^2 + 2\xi\omega_{\mathrm{n}}s + \omega_{\mathrm{n}}^2},\\ \frac{\overline{P}^{\mathrm{m}}(s)}{P_{\mathrm{load}}(s)} &= \frac{k\zeta R_{\mathrm{eff}}^{-1}}{s^2 + 2\xi\omega_{\mathrm{n}}s + \omega_{\mathrm{n}}^2},\end{aligned} \tag{21}$$

where the parameters k, ζ, ω_{n}, and ξ are given by

$$\begin{aligned} k &:= M_{\mathrm{eff}}^{-1}, \qquad & \zeta &:= \overline{\tau}^{-1}, \\ \omega_{\mathrm{n}} &:= \sqrt{\frac{R_{\mathrm{eff}}^{-1} + D_{\mathrm{eff}}}{\overline{\tau} M_{\mathrm{eff}}}}, \quad & \xi &:= \frac{1}{2}\frac{M_{\mathrm{eff}} + \overline{\tau}D_{\mathrm{eff}}}{\sqrt{\overline{\tau}M_{\mathrm{eff}}(R_{\mathrm{eff}}^{-1} + D_{\mathrm{eff}})}}. \end{aligned} \tag{22}$$

Substituting $P_{\mathrm{load}}(s) = \Delta P_{\mathrm{load}}/s$ in (21) (to model the load step at time $t = 0$), and taking the inverse Laplace transform assuming the system is underdamped, i.e., $0 < \xi < 1$, we get

$$\begin{aligned}\Delta\overline{\omega}(t) &= \Delta\overline{\omega}_{\mathrm{ss}}\Big(1 - \frac{\mathrm{e}^{-\xi\omega_{\mathrm{n}}t}}{\sqrt{1-\xi^2}}\big(\sin(\omega_{\mathrm{d}}t + \varphi) - \frac{\omega_{\mathrm{n}}}{\zeta}\sin(\omega_{\mathrm{d}}t)\big)\Big)\\ &=: f_{\Delta\overline{\omega}}(t)\Delta P_{\mathrm{load}}, \end{aligned} \tag{23}$$

$$\begin{aligned}\overline{P}^{\mathrm{m}}(t) &= \overline{P}^{\mathrm{m}}(0) + \Delta\overline{P}^{\mathrm{m}}_{\mathrm{ss}}\Big(1 - \frac{\mathrm{e}^{-\xi\omega_{\mathrm{n}}t}}{\sqrt{1-\xi^2}}\sin(\omega_{\mathrm{d}}t + \varphi)\Big)\\ &=: \overline{P}^{\mathrm{m}}(0) + f_{\overline{P}^{\mathrm{m}}}(t)\Delta P_{\mathrm{load}}, \end{aligned} \tag{24}$$

where the parameters ω_{d}, φ, $\Delta\overline{\omega}_{\mathrm{ss}}$, and $\Delta\overline{P}^{\mathrm{m}}_{\mathrm{ss}}$ are given by

$$\begin{aligned} \omega_{\mathrm{d}} &= \omega_{\mathrm{n}}\sqrt{1-\xi^2}, \quad \varphi = \cos^{-1}\xi, \\ \Delta\overline{\omega}_{\mathrm{ss}} &= -\frac{\Delta P_{\mathrm{load}}}{R_{\mathrm{eff}}^{-1} + D_{\mathrm{eff}}}, \quad \Delta\overline{P}^{\mathrm{m}}_{\mathrm{ss}} = \frac{R_{\mathrm{eff}}^{-1}\Delta P_{\mathrm{load}}}{R_{\mathrm{eff}}^{-1} + D_{\mathrm{eff}}}. \end{aligned} \tag{25}$$

Furthermore, (19) is a first-order differential equation with solution that can be expressed in closed form as

$$\begin{aligned}\overline{P}^{\mathrm{m}}_g(t) &= \overline{P}^{\mathrm{m}}_g(0) + \Delta\overline{P}^{\mathrm{m}}_{g,\mathrm{ss}}\Bigg(1 - \frac{\omega_{\mathrm{d}}\tau_g^{-1}}{\omega_{\mathrm{d}}^2 + \theta_g^2}\cdot\frac{\mathrm{e}^{-\xi\omega_{\mathrm{n}}t}}{\sqrt{1-\xi^2}}\\ &\quad\Big(\frac{\omega_{\mathrm{n}}}{\zeta}\cos(\omega_{\mathrm{d}}t) - \cos(\omega_{\mathrm{d}}t + \varphi)\\ &\quad + \frac{\theta_g}{\omega_{\mathrm{d}}}(\sin(\omega_{\mathrm{d}}t + \varphi) - \frac{\omega_{\mathrm{n}}}{\zeta}\sin(\omega_{\mathrm{d}}t))\Big)\Bigg)\\ &=: \overline{P}^{\mathrm{m}}_g(0) + f_{P^{\mathrm{m}}_g}(t)\Delta P_{\mathrm{load}}, \end{aligned} \tag{26}$$

where the parameters $\Delta\overline{P}^{\mathrm{m}}_{g,\mathrm{ss}}$ and θ_g are given by

$$\Delta\overline{P}^{\mathrm{m}}_{g,\mathrm{ss}} = -R_g^{-1}\Delta\overline{\omega}_{\mathrm{ss}} = \frac{R_g^{-1}\Delta P_{\mathrm{load}}}{R_{\mathrm{eff}}^{-1} + D_{\mathrm{eff}}}, \quad \theta_g = \tau_g^{-1} - \xi\omega_{\mathrm{n}}. \tag{27}$$

With the above, solving the first equation in (15), we get

$$\Delta\dot{\overline{\omega}}(t) = M_{\mathrm{eff}}^{-1}\left(\overline{P}^{\mathrm{m}}(t) - D_{\mathrm{eff}}\Delta\overline{\omega}(t) - P_{\mathrm{load}}(t)\right), \tag{28}$$

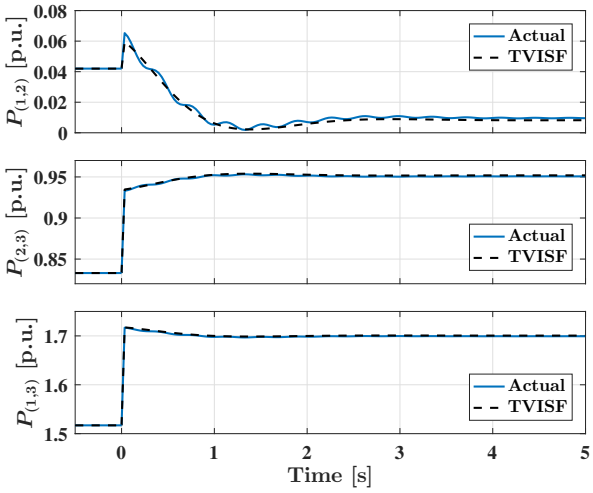

Fig. 3: Three-bus system: actual and predicted line flows due to 0.3 p.u. increase in active-power load at bus 3.

which can be substituted into (20) to yield

$$\begin{aligned}\overline{P}_g(t) &= \overline{P}^{\mathrm{m}}_g(t) + \left(M_g M_{\mathrm{eff}}^{-1}D_{\mathrm{eff}} - D_g\right)\Delta\overline{\omega}(t)\\ &\quad - M_g M_{\mathrm{eff}}^{-1}\left(\overline{P}^{\mathrm{m}}(t) - P_{\mathrm{load}}(t)\right). \end{aligned} \tag{29}$$

Due to the step change in load, for $t > 0$, $P_{\mathrm{load}}(t) = P_{\mathrm{load}}(0) + \Delta P_{\mathrm{load}}$. Substitute this along with (23), (24), and (26) into (29), we get

$$\begin{aligned}\overline{P}_g(t) &= \overline{P}^{\mathrm{m}}_g(0) - M_g M_{\mathrm{eff}}^{-1}\left(\overline{P}^{\mathrm{m}}(0) - P_{\mathrm{load}}(0)\right)\\ &\quad + f_{P^{\mathrm{m}}_g}(t)\Delta P_{\mathrm{load}} + \left(M_g M_{\mathrm{eff}}^{-1}D_{\mathrm{eff}} - D_g\right)f_{\Delta\overline{\omega}}(t)\Delta P_{\mathrm{load}}\\ &\quad - M_g M_{\mathrm{eff}}^{-1}\left(f_{\overline{P}^{\mathrm{m}}}(t) - 1\right)\Delta P_{\mathrm{load}}. \end{aligned} \tag{30}$$

Assuming that the system initially operates at synchronous frequency, i.e., $\Delta\overline{\omega}(0) = 0$, $\overline{P}^{\mathrm{m}}(0) = P_{\mathrm{load}}(0)$, and $\overline{P}^{\mathrm{m}}_g(0) = \overline{P}_g(0)$, (30) can be simplified as

$$\overline{P}_g(t) = \overline{P}_g(0) + \Delta\overline{P}_g(t) =: \overline{P}_g(0) + f_{P_g}(t)\Delta P_{\mathrm{load}}, \tag{31}$$

where

$$\begin{aligned}f_{P_g}(t) &= f_{P^{\mathrm{m}}_g}(t) + \left(M_g M_{\mathrm{eff}}^{-1}D_{\mathrm{eff}} - D_g\right)f_{\Delta\overline{\omega}}(t)\\ &\quad - M_g M_{\mathrm{eff}}^{-1}\left(f_{\overline{P}^{\mathrm{m}}}(t) - 1\right). \end{aligned} \tag{32}$$

In (32), time-domain functions $f_{P^{\mathrm{m}}_g}(t)$, $f_{\Delta\overline{\omega}}(t)$, and $f_{\overline{P}^{\mathrm{m}}}(t)$ can be readily extracted in closed form from (26), (23), and (24), respectively. With this, we achieve the aim in (6)–(7) albeit with the approximation that $\Delta P_g(t) \approx \Delta\overline{P}_g(t)$.

IV. Case Studies

In this section, we illustrate concepts presented in Sections II–III via numerical case studies.

A. Three-bus Test System

Consider the lossless three-bus system from Example 1. To predict the line active-power flows throughout the transient period following a load increase at bus 3, i.e., $\Delta P_3(t) = 0.3\,\mathrm{p.u.}$, $t > 0$, we begin by computing the time-varying

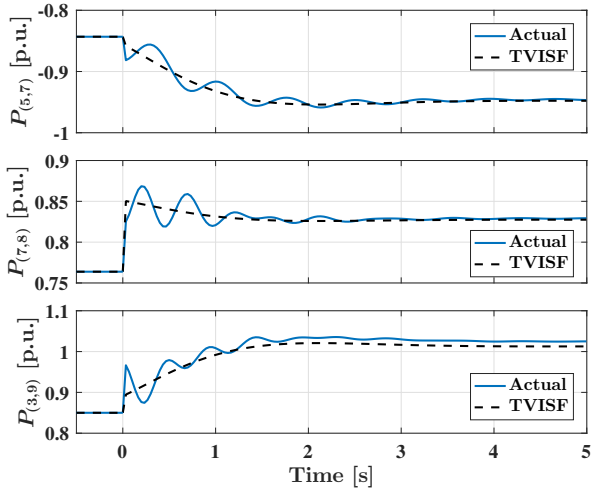

Fig. 4: WECC system: actual and predicted line flows due to $0.5\,$p.u. increase in active-power load at bus 6.

participation factors using (32). Then, the TVISFs in (6) allow us to map load disturbance contributions to line active-power flow variations via (7). Indeed, as shown in Fig. 3, the TVISFs not only capture the inertial- and governor-based response, but the dynamics across the entire transient period.

B. WECC Test System

Suppose generators in the WECC system are responding to a generation-load mismatch caused by a load increase at bus 6, i.e., $\Delta P_6(t) = 0.5\,$p.u., $t > 0$. Actual and predicted line flows on three lines are plotted in Fig. 4. We observe that the steady-state prediction errors are larger than those observed in Fig. 3. Specifically, the average prediction error over all lines is $0.0086\,$p.u., with a maximum error of $0.011\,$p.u., corresponding to line $(3, 9)$. As shown in Fig. 5, the average prediction error grows as the change in system losses (from pre- to post-disturbance steady state) increase due to varying load step changes.

V. Concluding Remarks

In this paper, we derive analytical closed-form expressions for time varying ISFs, which are valid throughout the post-contingency transient period. The utility of the proposed expressions in accurately predicting post-contingency active-power line flows was demonstrated via numerical case studies involving the WECC test system. Compelling avenues for future work include incorporating system losses, measurement-based ISFs using real-time measurements obtained from the system without relying on an offline model of the system, and location-cognizant aggregate-frequency models that consider the disturbance locational effect.

Appendix

A. Three-bus Test System Parameters

Synchronous generators are connected to buses 1 and 2, injecting $P_1 = 1.559\,$p.u. and $P_2 = 0.791\,$p.u., respectively. A constant-power load is connected to bus 3,

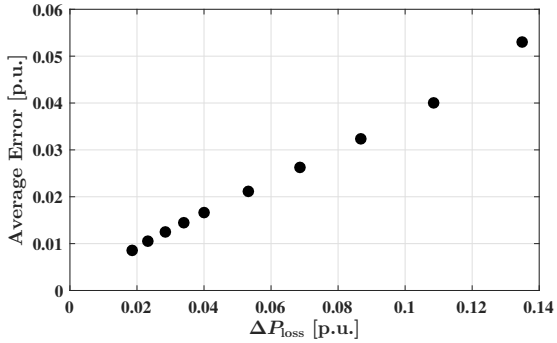

Fig. 5: WECC system: sensitivity of average error in line flow predictions with respect to change in system losses.

with active- and reactive-power injections $P_3 = -2.35\,$p.u. and $Q_3 = -0.5\,$p.u., respectively. Voltage magnitudes at buses 1 and 2 are regulated at $|V_1| = 1.04\,$p.u. and $|V_2| = 1.025\,$p.u., respectively. Transmission lines are modelled using lumped parameters, where $y_{12} = -\text{j}11.7647\,$p.u., $y_{12}^{\text{sh}} = \text{j}0.088\,$p.u., $y_{23} = -\text{j}6.2112\,$p.u., $y_{23}^{\text{sh}} = \text{j}0.153\,$p.u., $y_{13} = -\text{j}10.8696\,$p.u., and $y_{13}^{\text{sh}} = \text{j}0.079\,$p.u. Additionally, generator damping coefficients are $D_1 = D_3 = 10\,$p.u., inertial constants are $M_1 = 16\,$s and $M_2 = 6.02\,$s, droop coefficients are $R_1^{-1} = R_2^{-1} = 25\,$p.u., and governor time constants are $\tau_1 = \tau_2 = 0.5\,$s.

References

[1] A. J. Wood and B. F. Wollenberg, *Power Generation, Operation and Control*. New York: Wiley, 1996.

[2] M. D. Ilić and Q. Liu, *Toward Sensing, Communications and Control Architectures for Frequency Regulation in Systems with Highly Variable Resources*. New York, NY: Springer New York, 2012, pp. 3–33.

[3] P. W. Sauer, "On the formulation of power distribution factors for linear load flow methods," *IEEE Transactions on Power Apparatus and Systems*, vol. PAS-100, pp. 764–779, Feb 1981.

[4] P. W. Sauer, K. E. Reinhard, and T. J. Overbye, "Extended factors for linear contingency analysis," in *Proc. of the 34th Annual Hawaii International Conference on System Sciences*, Jan 2001, pp. 697–703.

[5] T. Güler, G. Gross, and M. Liu, "Generalized line outage distribution factors," *IEEE Transactions on Power Systems*, vol. 22, no. 2, pp. 879–881, May 2007.

[6] P. W. Sauer and M. A. Pai, *Power System Dynamics and Stability*. Upper Saddle River, NJ: Prentice-Hall, Inc., 1998.

[7] M. Lotfalian, R. Schlueter, D. Idizior, P. Rusche, S. Tedeschi, L. Shu, and A. Yazdankhah, "Inertial, governor, and AGC/economic dispatch load flow simulations of loss of generation contingencies," *IEEE Transactions on Power Apparatus and Systems*, vol. PAS-104, no. 11, pp. 3020–3028, Nov 1985.

[8] F. Milano, "An open source power system analysis toolbox," *IEEE Trans. on Power Systems*, vol. 20, no. 3, pp. 1199–1206, Aug 2005.

[9] P. M. Anderson and M. Mirheydar, "A low-order system frequency response model," *IEEE Transactions on Power Systems*, vol. 5, no. 3, pp. 720–729, 1990.

[10] D. Apostolopoulou, P. W. Sauer, and A. D. Domínguez-García, "Balancing authority area model and its application to the design of adaptive AGC systems," *IEEE Transactions on Power Systems*, vol. 31, no. 5, pp. 3756–3764, September 2016.

[11] S. S. Guggilam, C. Zhao, E. Dall'Anese, Y. C. Chen, and S. V. Dhople, "Engineering inertial and primary-frequency response for distributed energy resources," in *IEEE Conference on Decision and Control*, 2017. [Online]. Available: https://arxiv.org/abs/1706.03612